

Think Proprioceptively: Embodied Visual Reasoning for VLA Manipulation

Fangyuan Wang^{1,2} Peng Zhou³ Jiaming Qi⁴ Shipeng Lyu^{1,2} David Navarro-Alarcon¹ Guodong Guo²

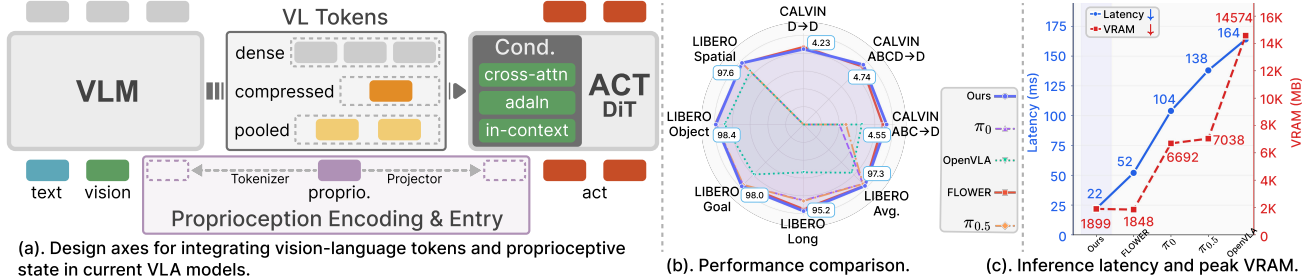


Figure 1. ThinkProprio tokenizes proprioception into the VLM space to guide early visual reasoning. This yields strong CALVIN/LIBERO performance with 15 % of visual tokens and 58 % lower latency than prior VLA policies.

Abstract

Vision-language-action (VLA) models typically inject proprioception only as a late conditioning signal, which prevents robot state from shaping instruction understanding and from influencing which visual tokens are attended throughout the policy. We introduce ThinkProprio, which converts proprioception into a sequence of text tokens in the VLM embedding space and fuses them with the task instruction at the input. This early fusion lets embodied state participate in subsequent visual reasoning and token selection, biasing computation toward action-critical evidence while suppressing redundant visual tokens. In a systematic ablation over proprioception encoding, state entry point, and action-head conditioning, we find that text tokenization is more effective than learned projectors, and that retaining roughly 15 % of visual tokens can match the performance of using the full token set. Across CALVIN, LIBERO, and real-world manipulation,

ThinkProprio matches or improves over strong baselines while reducing end-to-end inference latency over 50 %. Project page: <https://nicehiro.github.io/ThinkProprio>.

1. Introduction

Vision-language-action (VLA) models have emerged as a powerful paradigm for generalizable robot control because they translate visual observations and natural-language instructions into executable actions through large-scale pre-training (Zitkovich et al., 2023; Kim et al., 2025b; Black et al., 2024a). Yet most current VLA pipelines introduce proprioceptive signals late in the processing stack, couple them only weakly to perception, or ignore them entirely. Contact-rich manipulation depends not only on what is visible and what action is requested, but also on the robot’s embodiment, including its joint configuration and motion. This raises a basic design question: when a robot interprets what it sees and what to do, how can it better leverage physically grounded state to understand the task and environment?

A striking example is the evolution from π_0 (Black et al., 2024a), where proprioceptive state is encoded by a simple projector and fed to the action head, to $\pi_{0.5}$ (Intelligence et al., 2025), where proprioceptive state is tokenized as text and fed through the VLM encoder. $\pi_{0.5}$ achieves an 18 % improvement on the CALVIN (Mees et al., 2022) ABC→D benchmark, with average completion length increasing from 2.01 to 2.38. Although other changes are present, the change

¹Department of Mechanical Engineering, The Hong Kong Polytechnic University, Kowloon, Hong Kong ²Ningbo Institute of Digital Twin, Eastern Institute of Technology, Ningbo, China

³School of Advanced Engineering, Great Bay University, Dongguan, China ⁴College of Mechanical and Electrical Engineering, Northeast Forestry University, Harbin, China. Correspondence to:

David Navarro-Alarcon <dnavar@polyu.edu.hk>, Guodong Guo <gdguo@eitech.edu.cn>.

in proprioceptive encoding and entry point is distinctive and plausibly contributes to the gain.

However, in existing systems, such as $\pi_{0.5}$, the proprioception design is typically chosen jointly with vision-language aggregation and the token conditioning mechanism at the action head, which makes the functional role of proprioception difficult to isolate. Figure 1(a) and Table 1 show that modern VLA models vary along several coupled axes, and these choices trade expressivity against efficiency and information retention. Cross-attention conditioning (Reuss et al., 2025) is flexible but expensive, while pooled tokens (Huang et al., 2025) or compressed tokens (Li et al., 2024) reduce compute at the cost of spatial detail. For proprioception, learned projections preserve continuous values but must map into an embedding space that is not pretrained, whereas text tokenization (Intelligence et al., 2025) leverages the VLM text interface but discretizes continuous state.

We conduct a systematic study to uncouple design choices by varying vision-language aggregation, the conditioning mechanism, and proprioception encoding and entry. To our knowledge, this provides the first systematic comparison. Building on the view that proprioception should be explicitly provided and actively involved during task understanding, we introduce ThinkProprio. Unlike LightVLA, which uses instruction-guided token selection primarily to reduce computation (Jiang et al., 2025), ThinkProprio uses *joint* instruction-and-proprioception guidance to study how embodied state shapes which visual evidence is retained during reasoning. In this framing, task-relevant evidence consists of object-centric visual cues together with configuration-specific proprioceptive context, which is sufficient to drive action generation without relying on heavier conditioning pathways. On CALVIN ABC→D, ThinkProprio improves average completion length from 4.44 to 4.55, and on LIBERO it increases average success from 96.9 % to 97.3 %. Moreover, it reduces end-to-end inference latency by 58 %, from 52 ms to 22 ms on CALVIN ABC→D.

2. Related Works

VLA models integrate perception, language understanding, and action generation to execute language instructions (Din et al., 2025). Single-system approaches such as OpenVLA (Kim et al., 2025b) learn an end-to-end mapping in a unified token space, whereas dual-system architectures separate semantic processing from motor execution with a dedicated action head. Diffusion-based policies are a common choice for action generation (He et al., 2025a;b).

2.1. Task Understanding in VLA

Vision-Language Feature Extraction. VLA systems differ in how vision-language backbone outputs are presented to

Table 1. Taxonomy of VLA design along two modalities. For the vision-language stream, we categorize how tokens are aggregated and how the action head is conditioned on the backbone features. For proprioception, we categorize how state is encoded, where it enters the pipeline, and how it conditions the action head.

Model	Vision-Language		Proprioception	
	Token	Conditioning	Encoding	Conditioning
π_0	Dense	Cross-attn	MLP→ACT	Cross-attn
$\pi_{0.5}$	Dense	Cross-attn	Tokenized→VLM	Cross-attn
SmolVLA	Dense	Cross-attn	MLP→VLM	Cross-attn
FLOWER	Dense	Cross-attn	MLP→ACT	AdaLN
Dita	Dense	In-context	MLP→ACT	In-context
CogACT	Compressed	In-context	N/A	N/A
OTTER	Pooled	Cross-attn	MLP→ACT	Cross-attn
DiT-Blocks	Pooled	AdaLN	MLP→VLM	Cross-attn

the action head. Some methods pass dense token sets directly, as in π_0 (Black et al., 2024a), $\pi_{0.5}$ (Intelligence et al., 2025), and FLOWER (Reuss et al., 2025). This choice preserves fine-grained information but increases computation at the action head. Other methods apply token aggregation before control. CogACT (Li et al., 2024) reduces the token set through compression, and DiT-Block (Dasari et al., 2024), OTTER (Huang et al., 2025), and LightVLA (Jiang et al., 2025) use pooling-style reductions that connect to a broader literature on token reduction (Rao et al., 2021; Ryoo et al., 2021). Across these designs, the robot’s proprioceptive state is typically not part of the representation that drives which vision-language tokens are retained, even though robot configuration can change which scene elements are relevant for spatially grounded actions.

Proprioceptive Encoding and Entry. Prior work integrates proprioception with different encodings and entry points. $\pi_{0.5}$ encodes proprioception as text and prepends it to the VLM input sequence, which aligns it with pretrained token embeddings. GR00T-N1 (Bjorck et al., 2025) and SmolVLA (Shukor et al., 2025) instead use multilayer perceptrons to project proprioception into the VLM feature space, which increases representational flexibility but can introduce mismatch relative to pretrained token features. FLOWER (Reuss et al., 2025) conditions the action head directly on proprioceptive inputs, bypassing the backbone.

2.2. Conditioning Mechanisms

Following the taxonomy introduced by Diffusion Transformer (DiT) (Peebles & Xie, 2023), VLA commonly use three conditioning mechanisms that differ in how vision-language tokens and proprioception enter the action head.

In-context Conditioning. Dita (Hou et al., 2025) concatenates vision-language features and proprioceptive embeddings with the action sequence and processes in self-attention. In single-system VLA models (Kim et al., 2025b), vision and language features are embedded as tokens and provided as prefix context to a decoder-only Transformer,

enabling action generation via in-context conditioning.

Adaptive Layer Normalization (AdaLN). DiT-Block (Dasari et al., 2024) applies global modulation by predicting layer-wise scale and shift parameters from pooled vision-language features and using them to modulate normalization during action generation. FLOWER (Reuss et al., 2025) and MDT (Reuss et al., 2024) use action-space Global AdaLN-Zero conditioning with proprioception.

Cross-Attention. π_0 (Black et al., 2024a) and $\pi_{0.5}$ (Intelligence et al., 2025) condition action computation via block-wise cross-attention with causal masking used to preserve the action-generation ordering. FLOWER (Reuss et al., 2025) integrates multimodal features into its Flow Transformer through cross-attention. Cross-attention retains token-level access to visual and language context, at the cost of higher computation.

Our approach targets this interface explicitly by representing robot configuration in the VLM token space and using it together with the instruction to prioritize a compact set of task-relevant visual evidence. This yields state-aware, token-level conditioning via cross-attention while improving efficiency by reducing the conditioning tokens.

3. Method

As shown in Figure 2, we propose ThinkProprio, an architecture built on the principle of *think proprioceptively*. We first tokenize proprioception into the VLM embedding space. We then use instruction and proprioceptive tokens jointly to guide the selection of task-relevant visual patches. The resulting compact token sequence is processed by the VLM, and the action head conditions on the VLM features through cross-attention to generate actions. We formalize the setting in Section 3.1, describe proprioceptive encoding and physically grounded token selection in Section 3.2 and Section 3.3, and present the training objective in Section 3.4.

3.1. Problem Setup

We consider a dual-system VLA policy π_θ with a vision-language backbone and a separate action head. At timestep t , the policy receives an observation o_t comprising n RGB images (I_t^1, \dots, I_t^n) , a language instruction ℓ , and a proprioceptive state $q_t \in \mathbb{R}^p$ that encodes the robot’s current configuration, such as joint angles and end-effector pose.

We represent each modality with tokens. A vision encoder maps the images to patch embeddings, yielding vision tokens $H_v \in \mathbb{R}^{N_v \times D}$, where N_v is the total number of patches across the n views and D is the embedding dimension. The instruction ℓ is tokenized into language tokens $H_l \in \mathbb{R}^{N_l \times D}$, where N_l is the number of text tokens. The proprioceptive state is encoded into proprio tokens $H_p \in \mathbb{R}^{N_p \times D}$ via an

encoding function f_q .

The architecture comprises a vision-language backbone f_{VLM} , initialized from a pretrained VLM, and an action head f_{ACT} . The backbone maps the tokenized observation to conditioning features C , and the action head predicts a continuous action chunk $a_{t:t+\mathcal{H}}$ conditioned on C .

3.2. Proprioceptive State Encoding

We implement the proprioceptive encoding function f_q by discretizing continuous state values and reusing the VLM token embedding table. At time t , the proprioceptive state $q_t \in \mathbb{R}^p$ contains p scalar values. We discretize each value using uniform binning over a clipped range, where q_{\min} and q_{\max} denote scalar clipping bounds applied elementwise and B is the number of bins. For each element $q_{t,k}$ with $k \in \{1, \dots, p\}$, we compute the bin index

$$b_{t,k} = \left\lfloor \frac{\text{clip}(q_{t,k}, q_{\min}, q_{\max}) - q_{\min}}{q_{\max} - q_{\min}} \cdot (B - 1) \right\rfloor. \quad (1)$$

Let V denote the VLM vocabulary size. We map each bin index to one of the last B vocabulary token IDs using a reverse mapping, namely $\tau_{t,k} = V - 1 - b_{t,k}$. We then obtain the corresponding embeddings from the VLM token embedding table, $H_p = f_q(q_t) = \text{Embed}(\tau_t) \in \mathbb{R}^{N_p \times D}$, where $\tau_t = [\tau_{t,1}, \dots, \tau_{t,p}]$ and $N_p = p$. This tokenization places proprioception in the same embedding space as language, enabling state-aware visual conditioning via cross-modal attention without introducing an additional projection.

3.3. Physically Grounded Token Selection

We use the task instruction and the robot’s current proprioceptive state to guide VLM visual token selection, so that subsequent attention layers focus on embodiment-relevant evidence while operating on a shorter effective sequence.

Query generation and scoring. Let the guidance tokens be $H_q = [H_l; H_p] \in \mathbb{R}^{N_q \times D}$, which concatenate instruction and proprio tokens. We apply RMSNorm to obtain $\tilde{H}_v = \text{RMSNorm}(H_v)$ and $\tilde{H}_q = \text{RMSNorm}(H_q)$. Each visual token attends to the guidance tokens to form a physically grounded query:

$$Q = \text{softmax} \left(\frac{\tilde{H}_v \tilde{H}_q^\top}{\sqrt{D}} \right) \tilde{H}_q \in \mathbb{R}^{N_v \times D}. \quad (2)$$

We then compute a score matrix by matching normalized queries to normalized visual tokens:

$$S = \frac{\tilde{Q} \tilde{H}_v^\top}{\sqrt{D}} \in \mathbb{R}^{N_v \times N_v}, \quad (3)$$

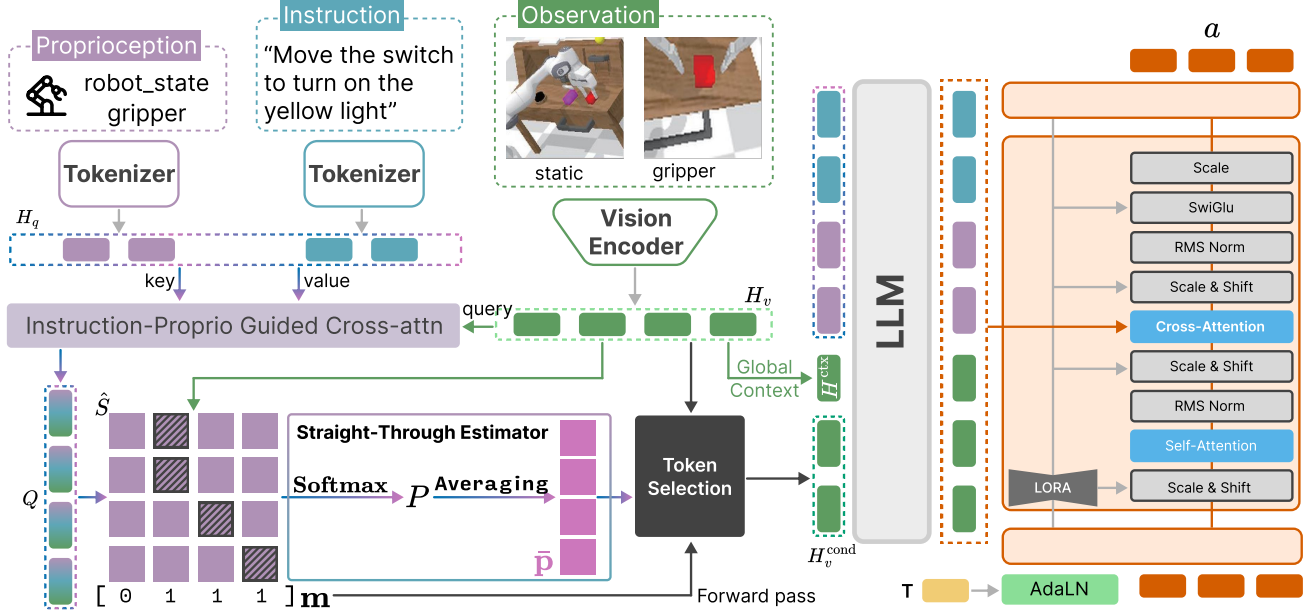


Figure 2. Overview of ThinkProprio. Proprioception is text-tokenized and combined with the instruction to guide visual token selection via cross-attention, retaining only task-relevant patches alongside a global context token. The compact token set is processed by the VLM, and the action head attends to the resulting features through cross-attention.

where $\hat{Q} = \text{RMSNorm}(Q)$. Each row of S scores all visual tokens for potential retention using a query grounded in instruction and proprioception.

Vote-based selection with annealed Gumbel noise. We use a vote-based discrete selection with a straight-through relaxation as one practical instantiation. We perturb the scores with i.i.d. Gumbel noise G and temperature α ,

$$\hat{S} = S + \alpha \cdot G, \quad (4)$$

where $G = -\log(-\log(U))$ and $U \sim \text{Unif}(0, 1)^{N_v \times N_v}$. As $\alpha \rightarrow 0$, the perturbation vanishes and selection becomes deterministic. We anneal α from α_{start} to α_{end} with a cosine schedule, which encourages exploration early in training and sharpens toward deterministic selection at convergence. Each row i of \hat{S} casts one vote by selecting the column index $j = \arg \max_k \hat{S}_{i,k}$. We retain all visual tokens that receive at least one vote, yielding a binary mask $\mathbf{m} = (m_1, \dots, m_{N_v})$ where $m_j = 1$ if token j receives at least one vote and $m_j = 0$ otherwise.

Straight-Through Estimation (STE). The mask \mathbf{m} gives the compact token set we need, but discrete selection has zero gradient with respect to the scores, which prevents the scoring computation from learning. We therefore use the straight-through estimator (STE), which uses hard selection in the forward pass while routing gradients through a differentiable surrogate in the backward pass. We form soft selection probabilities using the Gumbel-softmax relaxation,

$$P = \text{softmax}(\hat{S}/\alpha) \in \mathbb{R}^{N_v \times N_v}, \quad (5)$$

where each row of P is a distribution over visual tokens, i.e., P_{ij} is the relaxed probability that query i would cast its vote for token j . Averaging across rows gives a per-token expected selection probability,

$$\bar{\mathbf{p}} = \frac{1}{N_v} \sum_{i=1}^{N_v} P_{i,:} \in \mathbb{R}^{N_v}. \quad (6)$$

We combine hard and soft signals with an STE vector,

$$\mathbf{w} = \mathbf{m} + \bar{\mathbf{p}} - \text{sg}(\bar{\mathbf{p}}), \quad (7)$$

where $\text{sg}(\cdot)$ denotes stop-gradient. In the forward pass, \mathbf{w} evaluates to \mathbf{m} , while in the backward pass the gradient satisfies $\nabla_{\theta} \mathbf{w} = \nabla_{\theta} \bar{\mathbf{p}}$ because \mathbf{m} and $\text{sg}(\bar{\mathbf{p}})$ do not contribute gradients. The conditioned visual tokens is $H_v^{\text{cond}} = \text{diag}(\mathbf{w}) H_v$, which scales each token by its STE weight before retaining the selected subset in the forward computation. The dominant selector computation scales as $\mathcal{O}(N_v^2 D)$.

Global context token. We append a global context token that preserves coarse scene information:

$$H^{\text{ctx}} = W_c \left(\frac{1}{N_v} \sum_{i=1}^{N_v} H_{v,i} \right), \quad (8)$$

where $H_{v,i} \in \mathbb{R}^D$ denotes the i -th token of H_v . The final sequence $[H_v^{\text{cond}}; H^{\text{ctx}}]$ is forwarded to the VLM alongside proprio and language tokens.

3.4. Training Objective

The VLM processes the compact token sequence to produce fused conditioning features

$$C = f_{\text{VLM}}([H_v^{\text{cond}}; H^{\text{ctx}}; H_p; H_l]). \quad (9)$$

We train the action head with flow matching (Lipman et al., 2023). We sample a continuous flow time $T \sim \text{Unif}(0, 1)$ and construct a noised action chunk $\mathbf{a}_{t:t+\mathcal{H}}^T = (1 - T)\mathbf{a}_{t:t+\mathcal{H}} + T\epsilon$, where $\epsilon \sim \mathcal{N}(0, \mathbf{I})$. The action head conditions on C through cross-attention and also conditions on T as a global diffusion-time signal. Following FLOWER, we embed T and inject it into the action Transformer via global AdaLN-style modulation while cross-attending to C .

Under the linear interpolation above, the target velocity field is $\epsilon - \mathbf{a}_{t:t+\mathcal{H}}$. The action head predicts $v_\theta = f_{\text{ACT}}(\mathbf{a}_{t:t+\mathcal{H}}^T, T, C)$, and we optimize

$$\mathcal{L} = \mathbb{E}_{T, \epsilon} \left[\|v_\theta - (\epsilon - \mathbf{a}_{t:t+\mathcal{H}})\|^2 \right]. \quad (10)$$

The action head receives proprioception through the cross-attention over C since proprioception is tokenized and integrated into the VLM input.

4. Main Results

We evaluate ThinkProprio on two questions. First, does ThinkProprio improve long-horizon task performance over strong baselines on CALVIN and LIBERO? Second, can ThinkProprio reduce inference cost (latency and VRAM) without degrading performance?

4.1. Experimental Setup

Benchmarks. We evaluate on two simulation benchmarks. **CALVIN** (Mees et al., 2022) requires completing chains of five language-conditioned tasks. We use the ABC→D split by training on environments A, B, and C and testing on the unseen environment D. We report success rate at chain length range from 1 to 5, noted as LH-1 to LH-5 and the average completed chain length, noted as Avg. Len. on ABC→D, with additional results on ABCD→D and D→D provided in the Appendix. **LIBERO** (Liu et al., 2023) comprises four suites that probe complementary generalization axes: LIBERO-Spatial tests spatial relationship understanding, LIBERO-Object tests generalization to novel objects, LIBERO-Goal evaluates transfer across goal specifications, and LIBERO-Long targets long-horizon completion. We

report average success rate across the 10 tasks in each suite.

Proprioceptive state details. The proprioceptive state follows each benchmark’s robot interface. For CALVIN, we use a 15-dimensional state consisting of tool-center-point position and orientation in world coordinates, seven arm joint angles, gripper opening width, and a binary gripper action indicator. For LIBERO, we use a 9-dimensional state consisting of seven joint angles and a two-dimensional gripper position. We text-tokenize proprioception by discretizing each dimension into 256 bins over the range $[-3, 3]$.

Implementation and measurement. We implement ThinkProprio on top of FLOWER (Reuss et al., 2025), which uses Florence-2-Large as the vision-language model. The action head is a DiT with hidden dimension 1024, 18 layers, and 16 attention heads, with dropout 0.1 throughout the transformer. We train for 50k steps with AdamW using learning rate 2×10^{-5} , $\beta = (0.9, 0.95)$, and transformer weight decay 0.05. We use cosine learning-rate schedule defined over the same 50k steps. The noise scale α_t is cosine-annealed from 1.0 to 0.01 over training. We measure per-timestep inference latency and peak VRAM during evaluation on a single RTX 4090 GPU. All efficiency results use bfloat16 inference, process two camera views per timestep, and sample the diffusion action head for 4 steps. We report results averaged over 5 independent evaluation runs.

4.2. Baselines

We compare against recent baselines that reflect common VLA and long-horizon policy designs. On CALVIN, we compare to single-system VLAs such as OpenVLA (Kim et al., 2025b), which decodes actions via token-based action representations, as well as methods with a dedicated continuous-control action head, including GR-1 (Wu et al., 2024), RoboFlamingo (Li et al., 2023), π_0 (Black et al., 2024a), $\pi_{0.5}$ (Intelligence et al., 2025), and FLOWER (Reuss et al., 2025). We report π_0 and $\pi_{0.5}$ numbers from our own fine-tuning runs (marked with *) because official CALVIN ABC→D results are not provided. We also include FLOWER[†], which uses the additional external robot-data pretraining described in the FLOWER paper, and we treat it separately from our primary comparisons. ThinkProprio and our main FLOWER baseline do not use this additional external pretraining. We further compare to visual planning approaches, including SuSIE (Black et al., 2024b), VPP (Hu et al.), and Seer (Tian et al., 2024), which use intermediate predictions to structure multi-step behavior. On LIBERO, we additionally report strong OpenVLA variants and contemporaneous baselines, including OpenVLA-OFT (Kim et al., 2025a), COA-VLA (Li et al., 2025), and LightVLA (Jiang et al., 2025).

Table 2. Results on CALVIN ABC→D. Success rate (%) at each chain length and average completed chain length (Avg. Len.). *Finetuned by us; [†]with external pretraining. Best in **bold**.

Method	LH-1 ↑	LH-2 ↑	LH-3 ↑	LH-4 ↑	LH-5 ↑	Avg. Len. ↑
OpenVLA	91.3	77.8	62.0	52.1	43.5	3.27
GR-1	85.4	71.2	59.6	49.7	40.1	3.06
RoboFlamingo	82.4	61.9	46.6	33.1	23.5	2.47
π_0^*	70.0	48.0	37.0	28.0	18.0	2.01
$\pi_{0.5}^*$	71.0	56.0	45.0	37.0	29.0	2.38
SuSIE	87.0	69.0	49.0	38.0	26.0	2.69
VPP	95.7	91.2	86.3	81.0	75.0	4.29
Seer	96.3	91.6	86.1	80.3	74.0	4.29
FLOWER	99.3	96.0	90.3	82.3	75.5	4.44
FLOWER [†]	99.4	95.8	90.7	84.9	77.8	4.53
ThinkProprio	97.7	96.1	92.2	86.7	82.1	4.55

Table 3. Results on LIBERO benchmark suites. Average success rate (%) across 10 tasks per suite. Best is in **bold**.

Method	Spatial ↑	Object ↑	Goal ↑	Long ↑	Avg. ↑
OpenVLA	84.7	88.4	79.2	53.7	76.5
OpenVLA-OFT	97.6	98.4	97.9	94.5	97.1
COA-VLA	85.3	93.1	85.8	55.0	79.8
π_0	96.8	98.8	95.8	85.2	94.2
$\pi_{0.5}$	98.0	97.8	95.6	85.8	94.3
FLOWER	97.5	99.1	96.1	94.9	96.9
LightVLA	98.4	98.4	98.2	94.6	97.4
ThinkProprio	97.6	98.4	98.0	95.2	97.3

4.3. Task Performance

On CALVIN ABC→D (Table 2), success decreases as the chain length increases, consistent with compounding errors in long-horizon execution. ThinkProprio achieves the best Avg. Len. (4.55), narrowly improving over FLOWER[†] (4.53). The gain is most pronounced at the longest horizon: at LH-5, ThinkProprio reaches 82.1 % versus 77.8 % for FLOWER[†], which corresponds to an approximately 19 % relative reduction in failure rate. These results are consistent with the intuition that proprio-guided token selection helps retain interaction-relevant visual evidence as the robot configuration evolves. This trend also aligns with the $\pi_0 \rightarrow \pi_{0.5}$ comparison in Table 2, where incorporating proprioception into the VLM input improves Avg. Len. from 2.01 to 2.38. ThinkProprio further uses proprioception and instruction as guidance signals for visual token extraction and yields larger gains over a stronger baseline.

Table 3 shows that ThinkProprio is competitive with the strongest LIBERO baselines. LightVLA achieves the best overall average (97.4 %), while ThinkProprio is close (97.3 %) and achieves the best performance on LIBERO-Long (95.2 %). Relative to FLOWER, ThinkProprio improves LIBERO-Long from 94.9 % to 95.2 %, matching the CALVIN observation that proprioceptive guidance is most helpful on more temporally extended settings.

Table 4. Inference efficiency on CALVIN ABC→D (1000 evaluation steps, bfloat16). We report the mean number of visual tokens passed into the VLM per timestep, end-to-end per-timestep latency (ms), and peak VRAM (MB).

Method	Visual Tokens ↓	Latency ↓	VRAM ↓	Avg. Len. ↑
OpenVLA	256	164	14574	3.27
π_0	256	104	6692	2.01
$\pi_{0.5}$	256	138	7038	2.38
FLOWER	100	52	1848	4.44
ThinkProprio	15	22	1899	4.55

Table 5. Mean per-timestep latency breakdown (1000 evaluation steps, bfloat16) on CALVIN and LIBERO. Tokens denotes the mean number of retained visual patch tokens per timestep (kept/available).

Benchmark	Tokens	Vision	Selector	VLM	Action	Total
CALVIN	15/100	5.8	0.1	0.9	15.4	22.2
LIBERO	6/34	6.5	0.1	1.1	16.1	23.8

4.4. Computational Efficiency

Table 4 compares inference cost on CALVIN ABC→D. ThinkProprio keeps only 15 of the 100 available visual tokens per step on average, which shortens the effective sequence processed by both the VLM and the action head. In our implementation, the selector gathers the kept tokens, pads them within each batch to the maximum kept length, and supplies an attention mask. Despite the additional selector, ThinkProprio achieves lower end-to-end latency (22 ms vs. 52 ms for FLOWER). Peak VRAM increases slightly relative to FLOWER (1899 MB vs. 1848 MB) due to selector parameters, but remains far below OpenVLA (14 574 MB). Table 5 decomposes total latency into vision encoding, selector, VLM inference, and the diffusion action head, and it reports token counts as kept/available (15/100 on CALVIN and 6/34 on LIBERO). The selector remains fast in this regime because it scores short token sets (100 or 34 tokens), while the diffusion action head dominates runtime.

5. Ablation Studies

We ablate two key design choices, the proprioception encoding and entry point and the token-retention query signal, while keeping the VLM backbone, policy head, training recipe, and data fixed. We ask: First, which components drive the performance-latency trade-off relative to the FLOWER backbone? Second, under the same training setup, which proprioception encoding and entry point are most effective? Third, when reducing visual tokens, how do simple pooling baselines compare with query-guided retention that conditions on the instruction and robot state?

Table 6. Component ablation of ThinkProprio on CALVIN ABC→D. Latency is reported in milliseconds (ms).

Method variant	Avg. Len. \uparrow	Latency (ms) \downarrow
FLOWER	4.44	52
+Proprio tokens (tokenized)	4.48	55
+Physically grounded selection	4.35	20
+Physically grounded selection + H^{ctx}	4.55	22

Table 7. Comparison of proprioceptive integration strategies on CALVIN ABC→D. We vary the encoding and entry point; *Cond.* denotes how proprioception conditions the **action head**.

Encoding	Entry	Cond.	Avg. Len. \uparrow
None	—	—	4.44
MLP	ACT	AdaLN	4.44
MLP	VLM	Cross-attn	4.15
Tokenizer	VLM	Cross-attn	4.48

5.1. Component Ablation

Table 6 reports a controlled incremental ablation. Starting from FLOWER, we first add text-tokenized proprioception to the VLM input, then introduce physically grounded token selection to select visual patches before the VLM, and finally append the global context token H^{ctx} that summarizes the full visual input.

Adding proprio tokens slightly improves Avg. Len. from 4.44 to 4.48 while modestly increasing latency from 52 to 55. Introducing physically grounded selection sharply reduces latency to 20 by retaining a smaller visual token set, but it also reduces Avg. Len. to 4.35, which suggests that selection without an additional global summary can drop useful scene context. Appending H^{ctx} restores and improves performance to 4.55 with 22 ms latency, indicating that the global context token complements the selected patches by preserving coarse information that is not reliably captured by the retained subset.

5.2. Proprioceptive Encoding and Entry Point

Table 7 isolates proprioceptive integration by varying the encoding scheme and where state enters the model, while keeping the backbone and action head fixed. (1) **MLP-to-ACT** maps the continuous state vector directly into the action head and uses AdaLN to modulate generation. (2) **MLP-to-VLM** projects the state into a token that is concatenated with vision and language tokens at the VLM input. The action head then conditions on the resulting VLM features via cross-attention. (3) **Text-to-VLM** discretizes the continuous state into bins and retrieves corresponding token embeddings from the VLM vocabulary, again reaching the action head through cross-attention over VLM outputs.

The baseline taking vision and language as input, already

Table 8. Visual token retention ablation on CALVIN ABC→D. We compare pooling-based reductions to query-guided retention. We report the fraction of visual tokens retained; **bold** highlights the best method within each block.

Method	Tokens	Avg. Len. \uparrow
Mean pooled	1 %	4.20
Max pooled	25 %	4.33
Random	50 %	4.24
Query-guided ($H_q = H_l$)	13 %	3.40
Query-guided ($H_q = H_p$)	3 %	3.12
Query-guided ($H_q = H_l + H_p$)	15 %	4.55

achieves 4.44, consistent with images encoding many implicit state cues. MLP-to-ACT matches the no-proprio baseline at 4.44, suggesting limited benefit from late global modulation. Injecting an MLP-projected state token at the VLM input degrades performance to 4.15, consistent with a distribution mismatch relative to pretrained token embeddings. By contrast, text tokenization with VLM entry achieves the best result at 4.48, indicating that using the VLM’s native token interface is a more effective way to make state available for downstream action generation. Although discretization sacrifices some numerical precision, it offers two advantages: the resulting embeddings lie in a space the VLM was pretrained to process, and the proprioceptive tokens participate directly in the VLM’s reasoning over vision and language rather than being fused only at the action head.

5.3. Vision token retention

Table 8 compares pooling-based compression against query-guided retention. Pooling methods reduce tokens without instruction or proprioception dependent queries. Mean pooling averages all tokens into one, max pooling keeps the top- K tokens by a fixed score, and random sampling uniformly draws K tokens. Query-guided retention scores visual tokens against guidance tokens H_q and retains those selected by the voting mechanism (with H^{ctx} appended in all query-guided variants).

Among pooling baselines, max pooling achieves 4.33 with 25 % tokens. In query-guided retention, using only instruction guidance ($H_q = H_l$, LightVLA’s query source) or only proprioceptive guidance ($H_q = H_p$) performs poorly, which is consistent with selecting primarily object-related or robot-related vision patches. In contrast, combining both signals ($H_q = [H_l; H_p]$) achieves 4.55 with only 15 % tokens. These results suggest that physically grounded guidance from instruction and proprioception can help sustain long-horizon performance under aggressive token selection.

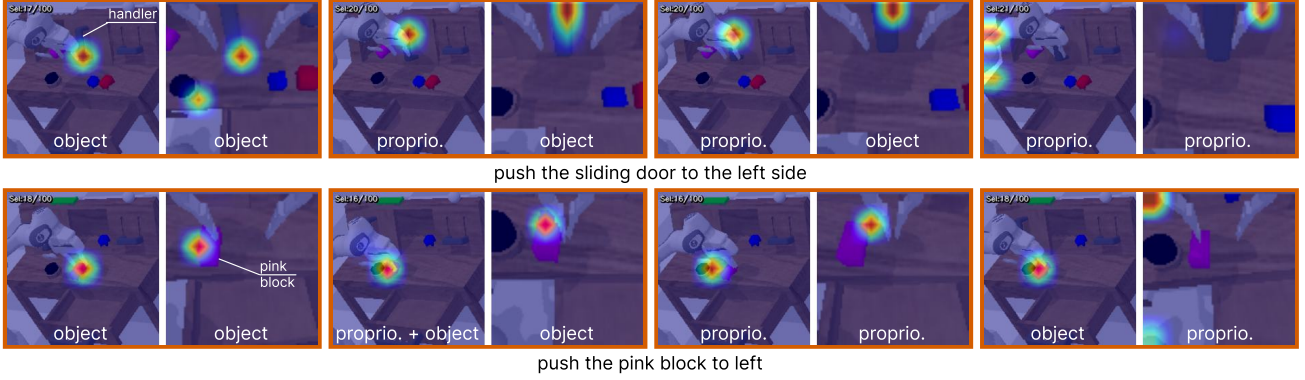


Figure 3. Token retention across four timesteps for two tasks, shown with paired static and wrist-mounted gripper views. Heatmaps visualize token retention scores, and labels indicate whether the retained tokens primarily focus on objects, proprioception, or both. The overlay Sel in each frame reports the number of retained tokens out of available visual tokens at that timestep.



Figure 4. Recovery behavior on a challenging stacking task. The policy requires more than 300 steps to stack the pink block on the smaller red support, and the heatmaps show persistent attention on the object and gripper as it repeatedly corrects the placement.

6. Analysis

6.1. Visualizing Physically Grounded Token Retention

To examine what visual evidence the physically grounded conditioning mechanism preserves, we project token-level retention scores onto the input images as heatmaps. Figure 3 shows two representative tasks over four timesteps each, with paired views from a static camera and a wrist-mounted gripper camera. The overlay in each frame (e.g., Sel:17/100) reports how many of the 100 available visual tokens are retained at that step. For each view, we label whether the retained tokens are predominantly object-centric, proprioception-centric, or reflect both foci. Across both tasks, the mechanism typically retains only 10 % to 20 % of tokens while still covering the interaction-relevant region, and the attended evidence transitions smoothly between object-centric and proprioception-centric focus as manipulation progresses.

When does proprioceptive guidance matter? We find that the balance between object-centric and proprioception-centric tokens depends on task phase. During *approach*, the selector emphasizes object tokens such as the drawer handle or the target block to support localizing the interaction target. During *contact and manipulation*, the focus shifts toward the gripper and arm, consistent with greater reliance on proprioceptive grounding under contact dynamics. Overall, this phase-dependent pattern indicates that joint instruction-proprioception guidance can modulate which

visual evidence is prioritized based on task context, whereas instruction-only selection lacks this pathway.

6.2. Recovery in Long-Horizon Tasks

We inspect challenging episodes to characterize policy behavior when task success requires extended correction. Figure 4 shows a stacking sequence that succeeds only after more than 300 steps. In the early frames, the policy picks up the pink block and places it roughly above the red support. Because the red block is smaller than the pink block, the placement induces slipping and tilting that prevents immediate success. In later frames, the selector heatmap remains concentrated on the pink block, gripper, and arm as the policy executes repeated micro-adjustments to stabilize the stack. This example suggests that even when the selector attends to the correct interaction region, completion can depend on contact dynamics that require many corrective steps or may exceed typical evaluation horizons.

7. Conclusion

ThinkProprio treats proprioception as a first-class modality throughout the pipeline and improves task performance on both CALVIN and LIBERO, with the largest gains in long-horizon evaluation. The strong vision-language baseline also in our ablations suggests that images already provide many implicit state cues, while proprioception can provide additional grounded information when integrated properly.

Additionally, we studied how proprioception should enter, be encoded in, and condition vision-language-action pipelines. In controlled ablations, discretizing proprioception into text tokens and mapping it into VLM token embeddings consistently outperformed MLP-based projectors, and physically grounded token selection guided by the instruction and proprioception enabled aggressive visual tokens reduction. Our real-world experiments in Appendix Section D provide preliminary validation that the approach transfers to physical hardware, though comprehensive real-world evaluation remains future work.

Impact Statement

This paper presents work whose goal is to advance the field of Machine Learning. There are many potential societal consequences of our work, none which we feel must be specifically highlighted here.

References

Bjorck, J., Castañeda, F., Cherniadev, N., Da, X., Ding, R., Fan, L., Fang, Y., Fox, D., Hu, F., Huang, S., et al. Gr00tn1: An open foundation model for generalist humanoid robots. *arXiv preprint arXiv:2503.14734*, 2025.

Black, K., Brown, N., Driess, D., Esmail, A., Equi, M., Finn, C., Fusai, N., Groom, L., Hausman, K., Ichter, B., Jakubczak, S., Jones, T., Ke, L., Levine, S., Li-Bell, A., Mothukuri, M., Nair, S., Pertsch, K., Shi, L. X., Tanner, J., Vuong, Q., Walling, A., Wang, H., and Zhilinsky, U. π_0 : A vision-language-action flow model for general robot control, 2024a. URL <https://arxiv.org/abs/2410.24164>.

Black, K., Nakamoto, M., Atreya, P., Walke, H. R., Finn, C., Kumar, A., and Levine, S. Zero-shot robotic manipulation with pre-trained image-editing diffusion models. In *The Twelfth International Conference on Learning Representations*, 2024b. URL <https://openreview.net/forum?id=c0chJTSbci>.

Chi, C., Xu, Z., Feng, S., Cousineau, E., Du, Y., Burchfiel, B., Tedrake, R., and Song, S. Diffusion policy: Visuomotor policy learning via action diffusion. *The International Journal of Robotics Research*, 44(10-11): 1684–1704, 2025.

Dasari, S., Mees, O., Zhao, S., Srirama, M. K., and Levine, S. The ingredients for robotic diffusion transformers. *arXiv preprint arXiv:2410.10088*, 2024.

Din, M. U., Akram, W., Saoud, L. S., Rosell, J., and Hussain, I. Vision language action models in robotic manipulation: A systematic review. *arXiv preprint arXiv:2507.10672*, 2025.

He, C., Camps, G. S., Liu, X., Schwager, M., and Sartoretti, G. Latent theory of mind: A decentralized diffusion architecture for cooperative manipulation. *arXiv preprint arXiv:2505.09144*, 2025a.

He, C., Liu, X., Camps, G. S., Sartoretti, G., and Schwager, M. Demystifying diffusion policies: Action memorization and simple lookup table alternatives, 2025b. URL <https://arxiv.org/abs/2505.05787>.

Hou, Z., Zhang, T., Xiong, Y., Duan, H., Pu, H., Tong, R., Zhao, C., Zhu, X., Qiao, Y., Dai, J., and Chen, Y. Dita: Scaling diffusion transformer for generalist vision-language-action policy. *arXiv preprint arXiv:2503.19757*, 2025.

Hu, Y., Guo, Y., Wang, P., Chen, X., Wang, Y.-J., Zhang, J., Sreenath, K., Lu, C., and Chen, J. Video prediction policy: A generalist robot policy with predictive visual representations. In *Forty-second International Conference on Machine Learning*.

Huang, H., Liu, F., Fu, L., Wu, T., Mukadam, M., Malik, J., Goldberg, K., and Abbeel, P. Otter: A vision-language-action model with text-aware visual feature extraction. *arXiv preprint arXiv:2503.03734*, 2025.

Intelligence, P., Black, K., Brown, N., Darpinian, J., Dhabalia, K., Driess, D., Esmail, A., Equi, M., Finn, C., Fusai, N., Galliker, M. Y., Ghosh, D., Groom, L., Hausman, K., Ichter, B., Jakubczak, S., Jones, T., Ke, L., LeBlanc, D., Levine, S., Li-Bell, A., Mothukuri, M., Nair, S., Pertsch, K., Ren, A. Z., Shi, L. X., Smith, L., Springenberg, J. T., Stachowicz, K., Tanner, J., Vuong, Q., Walke, H., Walling, A., Wang, H., Yu, L., and Zhilinsky, U. $\pi_{0.5}$: a vision-language-action model with open-world generalization, 2025. URL <https://arxiv.org/abs/2504.16054>.

Jiang, T., Jiang, X., Ma, Y., Wen, X., Li, B., Zhan, K., Jia, P., Liu, Y., Sun, S., and Lang, X. The better you learn, the smarter you prune: Towards efficient vision-language-action models via differentiable token pruning. *arXiv preprint arXiv:2509.12594*, 2025.

Kim, M. J., Finn, C., and Liang, P. Fine-tuning vision-language-action models: Optimizing speed and success, 2025a. URL <https://arxiv.org/abs/2502.19645>.

Kim, M. J., Pertsch, K., Karamcheti, S., Xiao, T., Balakrishna, A., Nair, S., Rafailov, R., Foster, E. P., Sanketi, P. R., Vuong, Q., et al. Openvla: An open-source vision-language-action model. In *Conference on Robot Learning*, pp. 2679–2713. PMLR, 2025b.

Li, J., Zhu, Y., Tang, Z., Wen, J., Zhu, M., Liu, X., Li, C., Cheng, R., Peng, Y., Peng, Y., and Feng, F. Coa-vla: Improving vision-language-action models via visual-textual chain-of-affordance, 2025. URL <https://arxiv.org/abs/2412.20451>.

Li, Q., Liang, Y., Wang, Z., Luo, L., Chen, X., Liao, M., Wei, F., Deng, Y., Xu, S., Zhang, Y., et al. Cogact: A foundational vision-language-action model for synergizing cognition and action in robotic manipulation. *arXiv preprint arXiv:2411.19650*, 2024.

Li, X., Liu, M., Zhang, H., Yu, C., Xu, J., Wu, H., Cheang, C., Jing, Y., Zhang, W., Liu, H., Li, H., and Kong, T. Vision-language foundation models as effective robot imitators. *arXiv preprint arXiv:2311.01378*, 2023.

Lipman, Y., Chen, R. T. Q., Ben-Hamu, H., Nickel, M., and Le, M. Flow matching for generative modeling, 2023. URL <https://arxiv.org/abs/2210.02747>.

Liu, B., Zhu, Y., Gao, C., Feng, Y., Liu, Q., Zhu, Y., and Stone, P. Libero: Benchmarking knowledge transfer for lifelong robot learning. *Advances in Neural Information Processing Systems*, 36:44776–44791, 2023.

Mees, O., Hermann, L., Rosete-Beas, E., and Burgard, W. Calvin: A benchmark for language-conditioned policy learning for long-horizon robot manipulation tasks. *IEEE Robotics and Automation Letters*, 7(3):7327–7334, 2022.

Peebles, W. and Xie, S. Scalable diffusion models with transformers. In *Proceedings of the IEEE/CVF international conference on computer vision*, pp. 4195–4205, 2023.

Rao, Y., Zhao, W., Liu, B., Lu, J., Zhou, J., and Hsieh, C.-J. Dynamicvit: Efficient vision transformers with dynamic token sparsification. *Advances in neural information processing systems*, 34:13937–13949, 2021.

Reuss, M., Yağmurlu, Ö. E., Wenzel, F., and Lioutikov, R. Multimodal diffusion transformer: Learning versatile behavior from multimodal goals. *arXiv preprint arXiv:2407.05996*, 2024.

Reuss, M., Zhou, H., Rühle, M., Yağmurlu, O. E., Otto, F., and Lioutikov, R. Flower: Democratizing generalist robot policies with efficient vision-language-flow models. In Lim, J., Song, S., and Park, H.-W. (eds.), *Proceedings of The 9th Conference on Robot Learning*, volume 305 of *Proceedings of Machine Learning Research*, pp. 3736–3761. PMLR, 27–30 Sep 2025. URL <https://proceedings.mlr.press/v305/reuss25a.html>.

Ryoo, M. S., Piergiovanni, A., Arnab, A., Dehghani, M., and Angelova, A. Tokenlearner: What can 8 learned tokens do for images and videos? *arXiv preprint arXiv:2106.11297*, 2021.

Shukor, M., Aubakirova, D., Capuano, F., Kooijmans, P., Palma, S., Zouitine, A., Aractingi, M., Pascal, C., Russi, M., Marafioti, A., et al. Smolvla: A vision-language-action model for affordable and efficient robotics. *arXiv preprint arXiv:2506.01844*, 2025.

Tian, Y., Yang, S., Zeng, J., Wang, P., Lin, D., Dong, H., and Pang, J. Predictive inverse dynamics models are scalable learners for robotic manipulation. *arXiv preprint arXiv:2412.15109*, 2024.

Wu, H., Jing, Y., Cheang, C., Chen, G., Xu, J., Li, X., Liu, M., Li, H., and Kong, T. Unleashing large-scale video generative pre-training for visual robot manipulation. In *The Twelfth International Conference on Learning Representations*, 2024. URL <https://openreview.net/forum?id=NxoFmGgWC9>.

Yue, Y., Wang, Y., Kang, B., Han, Y., Wang, S., Song, S., Feng, J., and Huang, G. Deer-vla: Dynamic inference of multimodal large language models for efficient robot execution. *Advances in Neural Information Processing Systems*, 37:56619–56643, 2024.

Zitkovich, B., Yu, T., Xu, S., Xu, P., Xiao, T., Xia, F., Wu, J., Wohlhart, P., Welker, S., Wahid, A., et al. Rt-2: Vision-language-action models transfer web knowledge to robotic control. In *Conference on Robot Learning*, pp. 2165–2183. PMLR, 2023.

Appendix for Think Proprioceptively

A. Training and Inference Details

A.1. Observations and Proprioceptive State

Image preprocessing follows the dataset transform configs. For CALVIN, both views are resized to 224×224 . During training, we apply RandomShiftsAug with padding 10 for `rgb_static` and padding 4 for `rgb_gripper`, then scale images to $[0, 1]$ and normalize with CLIP statistics. Validation disables RandomShiftsAug but keeps resize and normalization. For LIBERO, we use the same augmentation/normalization structure, resizing images to 112×112 .

For CALVIN, the proprioceptive state is `robot_obs` (15D), normalized using dataset statistics and with additional normalization of orientation entries. For LIBERO, we form a 9D proprio state by concatenating 7 joint values with the 2D gripper state. In both benchmarks, actions are 7D relative actions (`rel_actions`) scaled to $[-1, 1]$.

When ThinkProprio tokenizes proprioception for selection, each scalar is clipped to $[-3, 3]$ and discretized into 256 uniform bins. Bin indices are mapped to the last 256 token ids in the VLM vocabulary, and the corresponding embeddings are retrieved from the VLM input embedding table.

A.2. Pre-VLM Visual Token Selection Implementation

Our pre-VLM selector takes vision tokens $H_v \in \mathbb{R}^{B \times V \times D}$ and query embeddings (instruction and/or tokenized proprioception) and produces a shorter vision sequence for the VLM encoder. It generates per-vision queries and computes a score tensor of shape $[B, V, V]$, where each of the V queries casts a vote over the same V candidate vision tokens. During training, it adds Gumbel noise with an annealed scale, applies a softmax to obtain a differentiable voting distribution, and takes an argmax over the noisy scores to form hard votes. A vision token is kept if it receives at least one vote, and we use a straight-through indicator of the form $\mathbf{w} = \mathbf{m} + \mathbf{p} - \text{sg}(\mathbf{p})$ so that the forward pass uses hard retention while gradients flow through the soft indicator.

Importantly, unkept tokens are removed rather than zeroed. For each batch element, we gather the kept tokens into a variable-length sequence, multiply them by the corresponding indicator weights during training, pad within the batch to the maximum kept length M , and return an attention mask that marks real versus padded positions. We also append a learned global context token computed from the mean of the original vision tokens. Compute savings therefore come from running the VLM encoder and the action head on the shorter effective length M (with masking), not from masking dense sequences. The selector's dominant cost scales as $O(V^2D)$, which is small compared with dense transformer computations in VLM and action head.

A.3. Model Architecture

We build on FLOWER and use Florence-2-Large (microsoft/Florence-2-large) as the vision-language backbone. We fine-tune the model rather than freezing Florence parameters. A special token `<Flow>` is embedded and inserted to mark the conditioning boundary. We apply token dropout with probability 0.1 to the VLM encoder outputs during training.

The action generator is a rectified-flow / Diffusion Transformer. It uses hidden size 1024, 18 transformer layers, and 16 attention heads, with dropout 0.1 in attention, residual, and MLP blocks. The policy predicts an action chunk of length 10 (`act_window_size=10`), and executes it with chunked replanning every 10 environment steps (`multistep=10`).

A.4. Optimization Hyperparameters

We train end-to-end with AdamW using learning rate 2×10^{-5} , betas $(0.9, 0.95)$, and weight decay 0.05 applied to non-normalization and non-bias parameters (norm/bias parameters use zero weight decay). Training uses bf16-mixed precision. We use a tri-stage learning-rate schedule over 50k steps (matching `max_epochs=50` and `limit_train_batches=1000`): (i) linear warmup for 5% of steps from $0.1 \times \text{lr}$ to lr , (ii) constant hold for 10% of steps, and (iii) cosine decay for the remaining 85% to a final learning rate of $0.5 \times \text{lr}$. We additionally maintain an exponential moving average (EMA) of parameters with decay 0.999 and use EMA weights for evaluation.

Table 9. Training and optimization hyperparameters used across experiments.

Setting	Value
Optimizer	AdamW
Learning rate	2×10^{-5}
AdamW betas	(0.9, 0.95)
Weight decay	0.05 (no decay on norm/bias)
Total steps	50,000
LR schedule	cosine-decay
Warmup / hold / decay	0.05/0.10/0.85
Warmup start lr	$0.1 \times lr$
Final lr	$0.5 \times lr$
Precision	bf16-mixed
EMA decay	0.999
VLM token dropout	0.1
Action chunk length	10

Table 10. CALVIN ABC→D long-horizon success with architecture and proprioception-interface details. Tokens is the number of visual tokens per timestep when reported; Enc., Entry, and Cond. summarize the proprioception encoding, injection point (Backbone/VLM/ACT), and action-conditioning mechanism (“–” = not applicable or not reported).

Method	Architecture					Performance					
	Scale (B)	Backbone	Tokens ↓	Enc.	Entry	Cond.	LH-1 ↑	LH-2 ↑	LH-3 ↑	LH-4 ↑	Avg. Len. ↑
SuSIE	–	–	–	–	–	–	87.0	69.0	49.0	38.0	26.0
VPP	1.5	SVD+CLIP	–	–	–	–	95.7	91.2	86.3	81.0	75.0
Seer	0.3	ViT+CLIP	–	–	–	–	96.3	91.6	86.1	80.3	74.0
Llama-2	–	–	–	–	–	–	–	–	–	–	4.29
OpenVLA	7.7	DINOv2+SigLIP CLIP	256	–	–	–	91.3	77.8	62.0	52.1	43.5
GR-1	0.195	MAE-ViT OpenFlamingo	–	MLP	Backbone	In-context	85.4	71.2	59.6	49.7	40.1
RoboFlamingo	3	ViT	128	–	–	–	82.4	61.9	46.6	33.1	23.5
π_0^*	3.3	PaliGemma	512	MLP	ACT	Cross-attn	70.0	48.0	37.0	28.0	18.0
$\pi_{0.5}^*$	3.3	PaliGemma	512	Tokenized	VLM	Cross-attn	71.0	56.0	45.0	37.0	29.0
FLOWER	0.95	Florence-2-L	100	–	–	–	99.3	96.0	90.3	82.3	75.5
FLOWER [†]	0.95	Florence-2-L	100	MLP	ACT	AdaLN	99.4	95.8	90.7	84.9	77.8
ThinkProprio	0.95	Florence-2-L	15	Tokenized	VLM	Cross-attn	97.7	96.1	92.2	86.7	82.1
											4.55

A.5. Inference Settings and Measurement Protocol

At inference time, we run rectified-flow sampling with 4 steps (num_sampling_steps=4) per action chunk. The model predicts a 10-step chunk and replans every 10 environment steps. Inference is performed in bf16 and always uses both camera views.

CALVIN long-horizon evaluation follows the standard 5-subtask instruction-chain protocol: each subtask is given up to 360 environment steps, and we report success rates for completing 1 through 5 subtasks as well as the average successful sequence length. LIBERO evaluation follows the standard success-rate protocol over fixed rollouts per task with a maximum horizon of 520 environment steps; we report per-task success and suite averages.

For latency and VRAM profiling, we measure per-environment-step end-to-end inference time including vision encoding, the pre-VLM selector, the Florence encoder forward pass, and all diffusion sampling steps. We compute latency with CUDA synchronization to avoid asynchronous kernel overlap artifacts, and report the mean over a fixed number of inference steps (1000 steps in our efficiency tables). Peak VRAM is reported as the maximum allocated GPU memory during inference. All profiling numbers in the paper are collected on a single RTX 4090 GPU under the same bf16 and two-view settings as evaluation.

Table 11. CALVIN ABCD→D long-horizon success with architecture and proprioception-interface details. Tokens is the number of visual tokens per timestep when reported; Enc., Entry, and Cond. summarize the proprioception encoding, injection point (Backbone/VLM/ACT), and action-conditioning mechanism (“–” = not applicable or not reported).

Method	Architecture						Performance					
	Scale (B)	Backbone	Tokens ↓	Enc.	Entry	Cond.	LH-1 ↑	LH-2 ↑	LH-3 ↑	LH-4 ↑	LH-5 ↑	Avg. Len. ↑
Diff-P-CNN	0.32	–	–	–	–	–	86.3	72.7	60.1	51.2	41.7	3.16
RoboFlamingo	3.0	OpenFlamingo	–	–	–	–	96.4	89.6	82.4	74.0	66.0	4.09
	3.0	ViT	128	–	–	–	99.1	93.3	82.1	74.6	63.8	4.13
DeerVLA	3.0	OpenFlamingo	128	–	–	–	–	–	–	–	–	–
GR-1	0.195	MAE-ViT	–	MLP	Backbone	In-context	94.9	89.6	84.4	78.9	73.1	4.21
	0.95	GPT	–	–	–	–	–	–	–	–	–	–
FLOWER	0.95	Florence-2-L	100	–	–	–	98.9	96.7	93.9	90.2	85.5	4.62
FLOWER [†]	0.95	Florence-2-L	100	MLP	ACT	AdaLN	99.2	96.9	96.9	92.3	88.3	4.67
ThinkProprio	0.95	Florence-2-L	15	Tokenized	VLM	Cross-attn	99.5	97.2	96.6	92.3	88.5	4.74

Table 12. CALVIN D→D long-horizon success with architecture and proprioception-interface details. Tokens is the number of visual tokens per timestep when reported; Enc., Entry, and Cond. summarize the proprioception encoding, injection point (Backbone/VLM/ACT), and action-conditioning mechanism (“–” = not applicable or not reported).

Method	Architecture						Performance					
	Scale (B)	Backbone	Tokens ↓	Enc.	Entry	Cond.	LH-1 ↑	LH-2 ↑	LH-3 ↑	LH-4 ↑	LH-5 ↑	Avg. Len. ↑
MDT	–	–	–	–	–	–	93.7	84.5	74.1	64.4	55.6	3.72
RoboUniView	–	–	–	–	–	–	96.2	88.8	77.6	66.6	56.3	3.85
FLOWER [†]	0.95	Florence-2-L	100	MLP	ACT	AdaLN	97.4	92.4	86.9	81.3	74.9	4.35
ThinkProprio	0.95	Florence-2-L	14	Tokenized	VLM	Cross-attn	96.9	89.8	83.6	80.5	72.7	4.23

B. Additional Results for CALVIN Benchmark

B.1. Baseline Details

For the extended tables in this appendix, we report a small set of architectural attributes and group methods into three families to reduce sparsity: **Single-system** VLAs (a single model directly predicts actions), **Dual-system** VLAs (a VLM conditions a separate action generator), and **Non-VLM** planner/predictor baselines. For proprioception, we summarize the encoding (**Enc.**), entry point (**Entry**; VLM vs. action head), and the conditioning interface into the action head (**Cond.**; e.g., AdaLN vs. cross-attention). Tokens reports the number of visual tokens per timestep when explicitly specified. We use “–” when not applicable or not reported.

- **FLOWER** (Reuss et al., 2025) uses Florence-2-Large and conditions a flow-based action generator on the backbone’s intermediate vision-language token sequence via cross-attention. This dense token conditioning preserves fine-grained spatial and semantic information, but its compute scales with the number of conditioning tokens processed by the VLM and consumed by the action head. In the simulated settings reported in Reuss et al. (2025), including CALVIN ABC→D, FLOWER does not explicitly feed proprioception into the backbone; therefore, the proprioception fields are marked as “–” for FLOWER in our extended tables. FLOWER[†] injects a continuous proprio embedding into the action head via AdaLN.
- **Diff-P-CNN** (Diffusion Policy CNN; Chi et al. 2025) is a non-VLM diffusion policy that denoises actions conditioned on visual observations (two RGB views) and the instruction. In our taxonomy, it serves as a CNN-based diffusion baseline without an explicit VLM backbone or a token-level cross-attention interface between a VLM and a separate action head.
- **GR-1** (Wu et al., 2024) is a video-generative-pretrained causal Transformer policy. It encodes language with CLIP and images with an MAE-pretrained ViT, reduces patch tokens with a Perceiver resampler, and injects robot state via an MLP as part of the input token sequence. Actions are generated in-context from the sequence, so proprioception conditions control via self-attention rather than a separate action-head conditioning interface.
- **DeerVLA** (Yue et al., 2024) introduces dynamic early-exit for Flamingo-style multimodal LLM backbones to trade compute for performance. It pools the backbone hidden states and predicts actions with a lightweight temporal head (e.g., LSTM+MLP). The paper does not specify a consistent proprioception for the CALVIN results we cite, so we mark the proprioception columns as “–” when not explicitly stated.

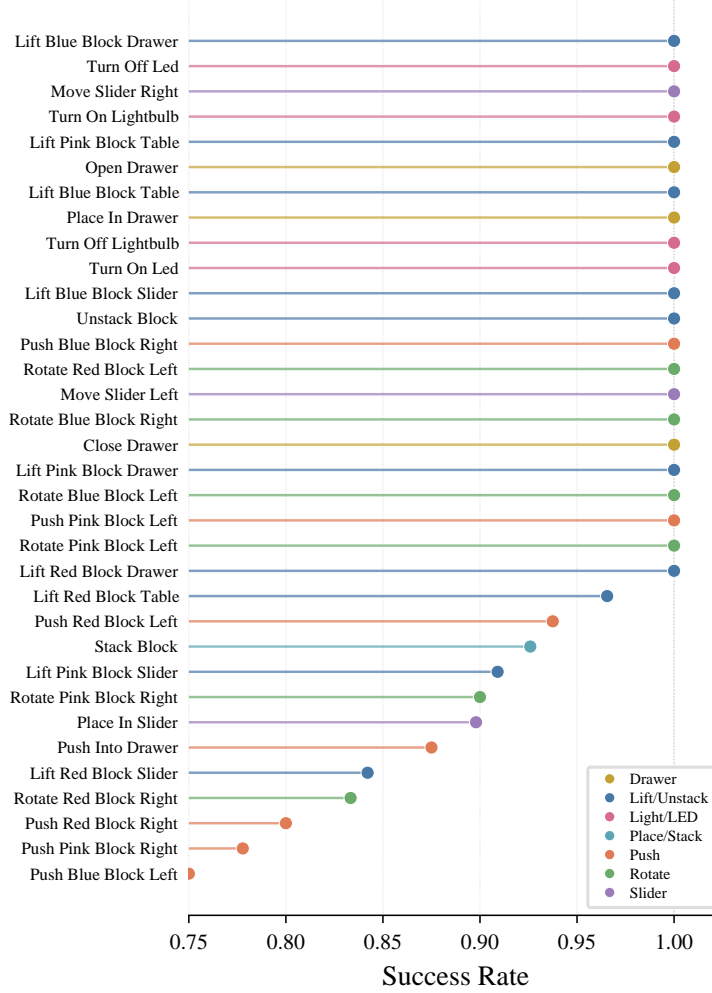


Figure 5. Per-subtask success rates for the 34 CALVIN long-horizon subtasks on task ABC→D. The horizontal lollipop plot reports success rate on a zoomed 0.75–1.00 axis, with colors indicating the subtask category.

- π_0 and $\pi_{0.5}$ (Black et al., 2024a; Intelligence et al., 2025) are dual-system VLAs that combine a PaliGemma VLM backbone with a flow-based action generator. In the full $\pi_{0.5}$ system, hierarchical inference is a key ingredient for long-horizon real-home tasks: it predicts a high-level semantic subtask as text and conditions low-level action generation on the predicted subtask. This hierarchical component is not implemented in the open-sourced $\pi_{0.5}$ variant we use. We therefore focus on the architectural distinction: how proprioception is represented and where it enters the network. We fine-tune π_0 and $\pi_{0.5}$ ourselves on CALVIN task ABC→D, and we reuse the reported results on LIBERO.
- **OpenVLA** (Kim et al., 2025b) is a 7B-scale open-source VLA that uses a Llama 2 language model backbone and a two-branch vision encoder combining DINOv2 and SigLIP features. OpenVLA is a single-system VLA that decodes actions autoregressively as discrete tokens. **OpenVLA-OFT** (Kim et al., 2025a) keeps the same OpenVLA backbone but introduces an optimized fine-tuning recipe that changes the action interface to improve speed and success, combining parallel decoding, action chunking, and a continuous action representation with a simple regression objective.
- **RoboFlamingo** (Li et al., 2023) adapts the Flamingo/OpenFlamingo vision-language fusion mechanism for robotic control. For the CALVIN numbers we report, the paper does not provide a consistent description of proprioception integration, so we mark the proprioception columns (Enc./Entry/Cond.) as “–” when not explicitly stated.
- **SuSIE** (Black et al., 2024b) is a planning-style baseline that uses intermediate predictions to structure multi-step behavior. We mark the unreported attributes in our extended tables as marked as “–”.

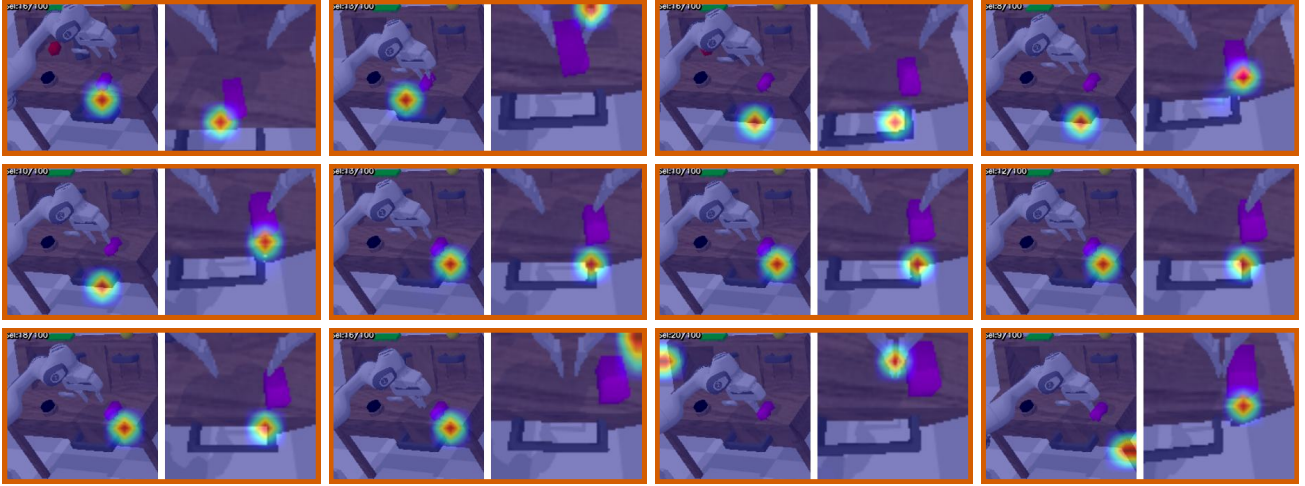


Figure 6. Failure case analysis on *Push Pink Block Right*. We show sequential timesteps from a representative failed rollout, with paired views from the static camera and the wrist-mounted gripper camera. Heatmaps overlay the selector’s token-retention scores (higher intensity indicates higher retention priority), illustrating where the model attends when deciding which visual evidence to preserve for action prediction. Despite repeated approaches, the end-effector does not maintain sustained contact with the pink block, leading to insufficient rightward displacement within the subtask horizon.

- **VPP** (Hu et al.) is a visual planning approach built on generative video prediction components. We mark non-applicable or unreported entries as “–”.
- **Seer** (Tian et al., 2024) is a predictive/planning baseline that uses intermediate predictions to guide control. Its CALVIN reporting does not provide a consistent mapping to our VLM-conditioning and proprio-injection fields, so we mark those attributes as “–” when unspecified.

B.2. CALVIN Long-Horizon Success Metrics

Tables 10–12 report CALVIN long-horizon performance for ABC→D, ABCD→D, and D→D. We report LH-1–LH-5, where LH- k is the success rate (%) of completing k consecutive subtasks in the five-subtask evaluation chain, and Avg. Len. is the mean number of consecutively completed subtasks. Table 10 additionally includes architecture and proprioception-interface details.

In the ABCD→D setting (more training data than ABC→D), ThinkProprio achieves an Avg. Len. of 4.74, compared to 4.62 for FLOWER and 4.67 for FLOWER[†]. The advantage is consistent at longer chains, where ThinkProprio reaches 88.5 on LH-5 versus 88.3 for FLOWER[†].

In D→D, ThinkProprio achieves an Avg. Len. of 4.23 and 72.7 on LH-5, which is slightly below FLOWER[†] (4.35 Avg. Len., 74.9 on LH-5). This comparison is not training-matched, since we train ThinkProprio on split D only, whereas FLOWER[†] uses additional multi-dataset pretraining before CALVIN fine-tuning (Appendix A (Pretraining Details) of Reuss et al. (2025)). The performance gap is therefore consistent with differences in pretraining and data diversity rather than isolating the effect of our method. Under the non-pretrained split-D setting, ThinkProprio still exceeds MDT (3.72 Avg. Len.) and RoboUniView (3.85 Avg. Len.), indicating a benefit over prior non-pretrained baselines in this regime.

Figure 5 breaks down performance by subtask for task ABC→D and shows that most subtasks achieve success rates close to 1.00. The remaining failures concentrate in a smaller set of subtasks that fall toward the lower end of the plotted range near 0.75. These lower-scoring cases appear predominantly in Push, Rotate, and Slider-related categories, suggesting these interactions are less uniformly reliable than the others.

B.3. Failed Case Analysis: Push Pink Block Right

We analyze *Push Pink Block Right* because it is one of the least reliable subtasks in the per-subtask breakdown: its success rate falls below 80% and is the second-lowest among the 34 CALVIN subtasks in Figure 5. Figure 6 visualizes a

Table 13. Extended LIBERO results with architecture and proprioception-interface details. Tokens is the number of visual patch tokens per timestep when reported. Enc., Entry, and Cond. summarize the proprioception encoding, the injection point (Backbone/VLM/ACT), and the action-conditioning mechanism (“–” = not applicable or not reported).

Method	Architecture						Performance				
	Scale (B)	Backbone	Tokens ↓	Enc.	Entry	Cond.	Spatial ↑	Object ↑	Goal ↑	Long ↑	Avg. ↑
OpenVLA	7.7	LLaMA-2	256	–	–	In-context	84.7	88.4	79.2	53.7	76.5
OpenVLA-OFT	7.7	LLaMA-2	512	–	–	In-context	97.6	98.4	97.9	94.5	97.1
COA-VLA	7	Qwen2-VL	–	MLP	Backbone	In-context	85.3	93.1	85.8	55.0	79.8
π_0^*	3.3	PaliGemma	512	MLP	ACT	Cross-attn	96.8	98.8	95.8	85.2	94.2
$\pi_{0.5}^*$	3.3	PaliGemma	512	Tokenized	VLM	Cross-attn	98.0	97.8	95.6	85.8	94.3
FLOWER	0.95	Florence-2-L	100	–	–	Cross-attn	97.5	99.1	96.1	94.9	96.9
LightVLA	7.7	LLaMA-2	78	–	–	In-context	98.4	98.4	98.2	94.6	97.4
ThinkProprio	0.95	Florence-2-L	6	Tokenized	VLM	Cross-attn	97.6	98.4	98.0	95.2	97.3

representative failure using token-retention heatmaps over both camera views, making it possible to inspect how attention over interaction-relevant regions evolves during execution.

A recurring pattern is that the gripper reaches the vicinity of the block but hesitates to commit to firm contact, or produces only a brief, shallow push before drifting away and re-approaching, rather than sustaining a consistent rightward push over multiple steps. This suggests that even visually simple pushing subtasks can be long-horizon and contact-sensitive: progress depends on maintaining contact while continuously correcting direction and force, yet the task provides no discrete closure event (unlike grasping) to stabilize behavior. Consistent with this interpretation, Figure 5 shows that multiple pushing subtasks remain noticeably below ceiling, which may reflect the difficulty of learning persistent, progress-accumulating behaviors when success is only weakly indicated until a final spatial condition is met.

C. Additional Results for the LIBERO Benchmark

C.1. Overview

LIBERO (Liu et al., 2023) is a simulated benchmark for language-conditioned imitation learning on tabletop manipulation with a Franka Panda arm. It is organized into four suites that target complementary forms of generalization. **LIBERO-Spatial** varies spatial relations, **LIBERO-Object** introduces novel objects, **LIBERO-Goal** evaluates transfer across goal specifications, and **LIBERO-Long** focuses on long-horizon multi-stage tasks. Each suite contains 10 tasks, and each task has 50 demonstrations. Observations include two RGB views from a static camera `agentview_rgb` and a wrist camera `eye_in_hand_rgb`, together with low-dimensional robot state. In our setup, proprioception is a 9D vector consisting of 7 joint angles and a 2D gripper state, and actions are 7D relative actions from `rel_actions`. **LightVLA** (Jiang et al., 2025) targets efficient VLA inference by pruning visual tokens with instruction-guided differentiable selection before attention-heavy computation. It builds on OpenVLA-OFT and adds a lightweight selector that uses the instruction as the query signal to score visual tokens and retain a subset for downstream processing.

C.2. Results

Figure 7 reports a task-level breakdown that makes clear where suite averages hide meaningful variation. In our setup, the selector operates over $H_v=34$ available visual tokens per step on LIBERO, and we report token counts as kept/available. Averaged over suites, we keep 5/34 (Spatial), 7/34 (Object), 3/34 (Goal), and 9/34 (Long), which matches the observation that the Long suite benefits from retaining more interaction-relevant evidence.

Spatial and Goal tasks are often near ceiling, so differences among strong methods are necessarily small and mainly appear in a small set of remaining failure cases. In contrast, Long shows a much wider performance spread, because failures more often arise from compounding errors over multi-stage execution, progressing from approach to grasp or contact, then manipulation, and finally placement. This long-horizon regime is where proprioceptive grounding matters most: as the robot’s configuration changes during interaction, the selector must continue to prioritize the end-effector neighborhood, contact region, and target object, rather than drifting toward visually salient but control-irrelevant regions. Consistent with this view, gains in suite-level averages are typically driven by improvements on a subset of harder long-horizon tasks, while performance on already-solved tasks remains essentially unchanged. Table 13 reports the corresponding extended summary in the same format as our CALVIN extended table, including suite-level success rates together with high-level architecture

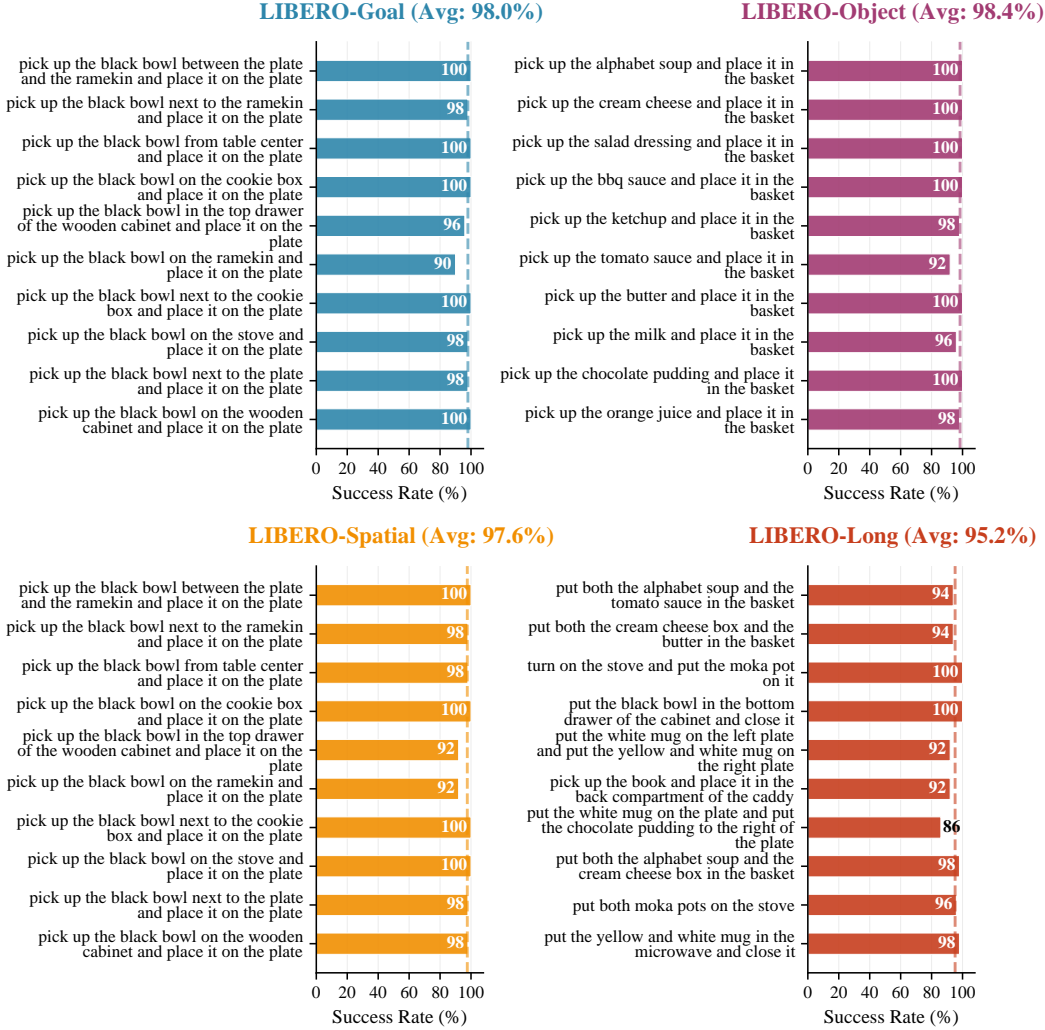


Figure 7. Per-task success rates (%) on LIBERO. For each task, we report the mean success over 20 evaluation rollouts for each method, with tasks grouped by suite (Spatial, Object, Goal, Long). This task-level view complements suite averages by revealing which individual tasks drive method differences, and it shows that LIBERO-Long exhibits the widest spread, making it the most diagnostic suite for compounding errors in multi-stage execution.

attributes and the proprioception interface.

D. Real-World Experiments

D.1. Hardware Setup and Sensing

As shown in Figure 8, we evaluate on a real tabletop setup using an xArm robotic arm with a parallel-jaw gripper. The policy observes two synchronized RGB streams from Intel RealSense D455 cameras. One camera provides a third-person static view of the workspace, and the other is rigidly mounted on the gripper to provide a wrist view. This two-view sensing matches our simulated interface with static and gripper views, and it reduces occlusions during grasping and placement.

We evaluate a compact task suite with two categories, **Pick-Place** and **Push**, as listed in Table 14. All tasks are single-instruction, single-goal tabletop manipulation with common objects and simple receptacles or targets, including plates and bowls. We collect 50 real-world trajectories via teleoperation across the suite and fine-tune from a checkpoint pretrained on the CALVIN benchmark. We keep the same observation interface, which combines the two RGB views with proprioception, and we keep the same action parameterization as in simulation to minimize real-to-sim interface mismatch.



Figure 8. Real-world evaluation setup with an xArm arm and a parallel-jaw gripper. Two Intel RealSense D455 RGB cameras provide a third-person static view of the workspace and a wrist view rigidly mounted on the gripper.

Table 14. Real-world evaluation tasks and instructions. The suite includes four Pick-Place tasks and four Push tasks, each specified by a single instruction that names the object and the target receptacle or goal relation.

ID	Category	Instruction
T01	Pick-Place	Pick up the banana and place it on the green plate.
T02	Pick-Place	Pick up the carrot and put it in the white bowl.
T03	Pick-Place	Pick up the orange and place it on the white plate.
T04	Pick-Place	Pick up the donut and put it in the white bowl.
T05	Push	Push the carrot next to the white bowl.
T06	Push	Push the banana next to the green plate.
T07	Push	Push the orange next to the white plate.
T08	Push	Push the donut next to the banana.

Our real-world evaluation is intentionally limited in scope and is not designed to provide a comprehensive measure of real-world performance. Since the underlying base model, Flower, is already strong on real-world tasks, we expect our approach to inherit much of this capability, although we do not claim broad real-world generalization from the limited evidence presented here. The main focus of this paper is improving the efficient use of proprioceptive information rather than maximizing scores on real-world benchmarks. We therefore include the real-world task primarily as a sanity check that verifies the full system can run end to end and produce coherent behavior under real sensor inputs and actuation in a physical setting. This evaluation serves to validate feasibility and basic robustness, while leaving extensive real-world benchmarking to future work.

D.2. Results

Table 15 reports success rates for FLOWER and ThinkProprio on the real-world suite. We run 20 trials per task and aggregate results over four tasks per category, which gives 80 trials per category and 160 trials overall. Both methods perform reliably on this suite, and ThinkProprio improves over FLOWER in both Pick-Place and Push. This margin is consistent with the idea that state-aware evidence selection is most helpful when execution depends on maintaining contact and recovering from small deviations. Figure 9 provides representative rollouts, and more challenging variants with heavier occlusions, tighter placement tolerances, or longer multi-stage tasks may further differentiate methods.

Figure 9 shows representative real-world rollouts for both FLOWER and ThinkProprio from the third-person static camera and the wrist-mounted gripper camera. The examples cover both Pick-Place and Push tasks. They illustrate the progression from approach to grasp or contact and then to placement or object displacement, and they show how the static and wrist views together preserve visibility of the end-effector and target objects when one view is occluded.

Table 15. Real-world manipulation success rates in % on the eight-task suite. We run 20 trials per task.

Method	Pick-Place	Push	Overall Avg.
FLOWER	88.8	86.2	87.5
ThinkProprio	92.5	90.0	91.3



Pick up the carrot and put it in the white bowl.



Pick up the donut and put it in the white bowl.



Push the donut next to the banana.



Push the orange next to the white plate.

Figure 9. Representative real-world rollouts for ThinkProprio on Pick-Place and Push tasks. We show frames from the third-person static camera and the wrist-mounted gripper camera to illustrate approach, grasp or contact, and placement or object displacement under partial occlusions.